Supporting Information

Insights into Crystal Structure and Diffusion of Biphasic $Na_2Zn_2TeO_6$

Xinyu Li[1*], Federico Bianchini[1], Julia Wind[1], Christine Pettersen[1], David Wragg[1], Ponniah Vajeeston[1], Helmer Fjellvåg[1*]

[1]Department of Chemistry and Center for Materials Science and Nanotechnology, University of Oslo, Norway

[*]Corresponding author: xinyu.li@smn.uio.no, helmer.fjellvag@kjemi.uio.no

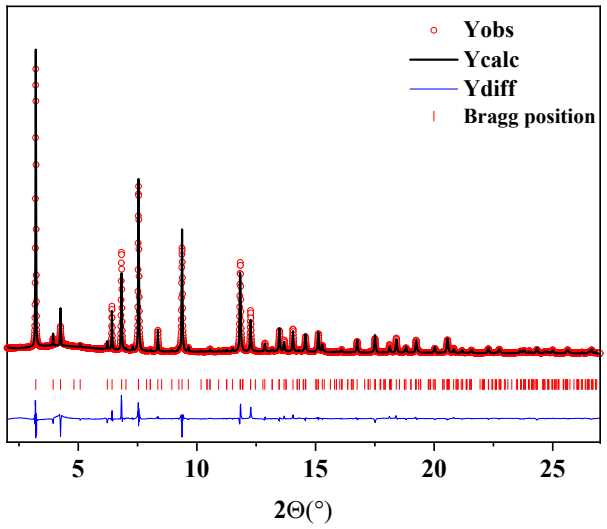

Figure S1: Rietveld refinement against SPXRD data of NZTO900, λ = 0.3149 Å. The experimental pattern is shown in red, calculated pattern in black, the difference between experimental and calculated curves in blue. Bragg positions of P2-type phase are in red.

Table S1: Crystallographic information obtained from Rietveld refinement against SPXRD data of NZTO900. P2-type phase in space group $P6_322$ (No.182), $a = b = 5.2880(1)$ and $c = 11.2388(2)$ Å, $V = 271.17(1)$ Å^3. $R_{wp} = 6.38\%$, $R_{exp} = 14.61\%$, GOF = 0.44.

Atom	Wyckoff Symbol	Coordinates			B_{iso} (Å^2)	Occupancy (this work)
		x	*y*	*z*		
Na1	6*g*	0.634(3)	0	0	2.1(2)	0.444(5)[c]
Na2	2*a*	0	0	0	2.1(2)	0.11(2)[c]
Na3	4*f*	1/3	2/3	0.506(2)	2.1(2)	0.28(1)[c]
O	12*i*	0.326(2)	0.326(2)	0.6500(3)	1.5(1)	1
Zn1	2*b*	0	0	1/4	1.00(4)	1
Zn2	2*d*	1/3	2/3	3/4	1.00(4)	1
Te	2*c*	1/3	2/3	1/4	1.00(4)	1

13 structure-related parameters for P2-type phase including lattice parameters, atomic coordinates, B_{iso} and Na site occupancies were refined; [c]a constraint of total occupancy across different Na sites was applied to the refinement according to stoichiometric value for Na.

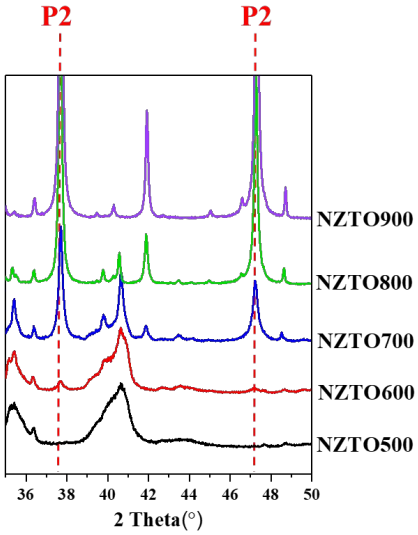

Figure S2: Enlarged 2θ range of 35-50° for PXRD patterns of NZTO500-900, λ = 1.5406 Å. The red dash lines indicate characteristic peaks for P2-type phase.

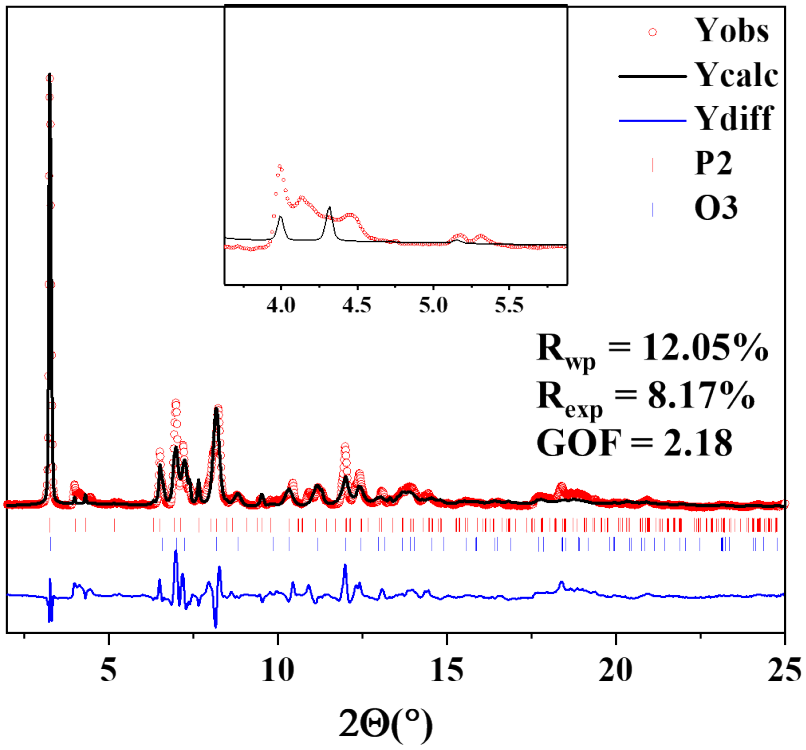

Figure S3: Rietveld refinement against SPXRD data of NZTO700 based on space group *R-3m*, λ = 0.319089 Å (inset: enlargement of 2θ range of 3.2 to 5.8°). The experimental pattern is shown in red, calculated pattern in black, the difference between experimental and calculated curves in blue. Bragg positions of P2 and O3-type phases are in red and blue, respectively.

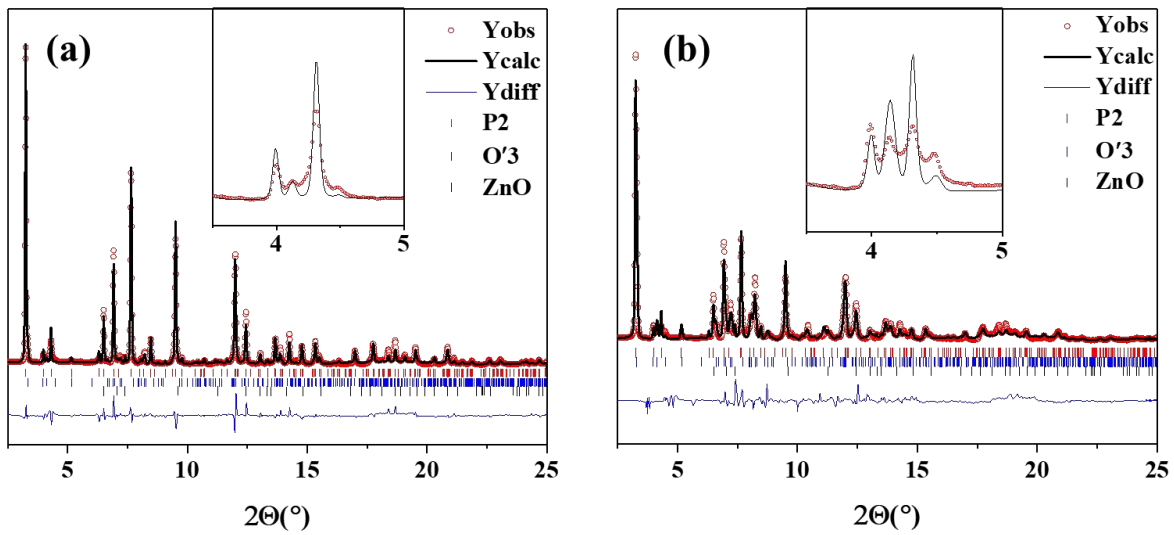

Figure S4: Rietveld refinements against SPXRD data of (a) NZTO800 and (b) NZTO700 based on O'3_model_1 (Inset: enlargement of 2θ range of 3.5 to 5°). The experimental patterns are shown in red, calculated patterns in black, the difference between experimental and calculated curves in blue. Bragg positions of P2, O'3-type phases and impurity ZnO are in red, blue and black, respectively. Wavelength (λ) for both SPXRD patterns is 0.319089 Å.

Table S2: Crystallographic information for P2 and O'3-type NZTO obtained from Rietveld refinement against SPXRD data of NZTO800. P2-type phase in space group *P6₃22* (No.182), $a = b = 5.2831(2)$ and $c = 11.2366(6)$ Å, $V = 271.62(2)$ Å^3; O'3-type phase (based on O'3_model_1) in space group *C2/m* (*No*.12), $a = 5.350(4)$, $b = 9.224(6)$ and $c = 5.814(3)$ Å, $\beta = 109.21(5)°$, $V = 271.0(3)$ Å^3. $R_{wp} = 10.13\%$, $R_{exp} = 8.38\%$, GOF = 1.21.

Atom	Wyckoff Symbol	Coordinates			B_{iso} (Å^2)	Occupancy
		x	*y*	*z*		
P2-type phase (~92%)						
Na1	6*g*	0.652(8)	0	0	2.1[a]	0.451(9)[c]
Na2	2*a*	0	0	0	2.1[a]	0.05(3)[c]
Na3	4*f*	1/3	2/3	0.504(4)	2.1[a]	0.30(2)[c]
O1	12*i*	0.339(3)	0.335(3)	0.6512(6)	1.5[a]	1
Zn1	2*b*	0	0	1/4	1.0[a]	1
Zn2	2*d*	1/3	2/3	3/4	1.0[a]	1
Te1	2*c*	1/3	2/3	1/4	1.0[a]	1
O'3-type phase (~6%)						
Na1	4*h*	0	0.181[a]	1/2	2.1[a]	1
O1	8*j*	0.197[a]	0.166[a]	0.209[a]	1.5[a]	1
O2	4*i*	0.76[a]	0	0.17[a]	1.5[a]	1
Zn1	4*g*	0	0.668[a]	0	1.0[a]	1
Te1	2*a*	0	0	0	1.0[a]	1

[a]B_{iso} values are fixed at values obtained from NZTO900 refinement; [a] atomic coordinates in O'3-type phase are fixed according to NZTO700 refinement based on O'3_model_1; 10 structure-related parameters for P2-type phase including lattice parameters, atomic coordinates and Na site occupancies were refined; lattice parameters for O'3-type phase were refined; [c]a constraint of total occupancy across different Na sites was applied to the refinement according to stoichiometric value for Na.

Table S3: Crystallographic information for P2 and O'3-type NZTO obtained from Rietveld refinement against SPXRD data of NZTO700. P2-type phase in space group $P6_322$ (*No.*182), $a = b = 5.2747(4)$ and $c = 11.242(2)$ Å, $V = 270.86(7)$ Å^3; O'3-type phase (based on O'3_model_1) in space group $C2/m$ (*No*.12), $a = 5.317(2)$, $b = 9.179(3)$ and $c = 5.857(2)$ Å, $\beta = 109.13(3)°$, $V = 270.1(2)$ Å^3. $R_{wp} = 11.15\%$, $R_{exp} = 8.16\%$, GOF = 1.37.

Atom	Wyckoff Symbol	Coordinates			B_{iso} (Å^2)	Occupancy
		x	*y*	*z*		
P2-type phase (~54%)						
Na1	6*g*	0.61(1)	0	0	2.1[a]	0.43(2)[c]
Na2	2*a*	0	0	0	2.1[a]	0.00(6)[c]
Na3	4*f*	1/3	2/3	0.462(6)	2.1[a]	0.35(4)[c]
O1	12*i*	0.352(6)	0.359(6)	0.652(1)	1.5[a]	1
Zn1	2*b*	0	0	1/4	1.0[a]	1
Zn2	2*d*	1/3	2/3	3/4	1.0[a]	1
Te1	2*c*	1/3	2/3	1/4	1.0[a]	1
O'3-type phase (~44%)						
Na1	4*h*	0	0.181(6)	1/2	2.1[a]	1
O1	8*j*	0.197(7)	0.166(9)	0.209(5)	1.5[a]	1
O2	4*i*	0.76(1)	0	0.17(1)	1.5[a]	1
Zn1	4*g*	0	0.668(2)	0	1.0[a]	1
Te1	2*a*	0	0	0	1.0[a]	1

[a]B_{iso} values are fixed at values obtained from NZTO900 refinement; 10 structure-related parameters for P2-type phase including lattice parameters, atomic coordinates and Na site occupancies were refined; 10 structure-related parameters for O'3-type phase including lattice parameters and atomic coordinates were refined; [c]a constraint of total occupancy across different Na sites was applied to the refinement according to stoichiometric value for Na.

Table S4: Crystallographic information for P2 and O'3-type NZTO obtained from Rietveld refinement against SPXRD data of NZTO800. P2-type phase in space group $P6_322$ (*No.*182), $a = b = 5.2831^a$ and $c = 11.2366^a$ Å, $V = 271.62^a$ Å^3; O'3-type phase (based on O'3_model_2) in space group $C2/m$ (*No.*12), $a = 5.353(3)$, $b = 9.227(5)$ and $c = 5.810(3)$ Å, $\beta = 109.22(4)°$, $V = 271.0(3)$ Å^3. $R_{wp} = 10.04\%$, $R_{exp} = 8.35\%$, GOF = 1.20.

Atom	Wyckoff Symbol	Coordinates			B_{iso} (Å^2)	Occupancy
		x	*y*	*z*		
P2-type phase (~92%)						
Na1	6*g*	0.652[a]	0	0	2.1[a]	0.451[a]
Na2	2*a*	0	0	0	2.1[a]	0.05[a]
Na3	4*f*	1/3	2/3	0.504[a]	2.1[a]	0.30[a]
O1	12*i*	0.339[a]	0.335[a]	0.6512[a]	1.5[a]	1
Zn1	2*b*	0	0	1/4	1.0[a]	1
Zn2	2*d*	1/3	2/3	3/4	1.0[a]	1
Te1	2*c*	1/3	2/3	1/4	1.0[a]	1
O'3-type phase (~6%)						
Na1	2*d*	0	1/2	1/2	2.1[a]	0.59[a]
Na2	4*h*	1/2	0.33[a]	1/2	2.1[a]	0.71[a]
O1	8*j*	0.221[a]	0.830[a]	0.214[a]	1.5[a]	1
O2	4*i*	0.26[a]	1/2	0.20[a]	1.5[a]	1
Zn1	4*g*	0	2/3	0	1.0[a]	0.94[a]
Zn2	2*a*	0	0	0	1.0[a]	0.12[a]
Te1	2*a*	0	0	0	1.0[a]	0.88[a]
Te2	4g	0	2/3	0	1.0[a]	0.06[a]

[a]B_{iso} values are fixed at values obtained from NZTO900 refinement; [a]structure-related parameters for P2-type phase are fixed according to the NZTO800 refinement based on O'3_model_1; [a]structure-related parameters for O'3-type phase are fixed according to NZTO700 refinement based on O'3_model_2; lattice parameters for O'3-type phase are refined; [c]a constraint of total occupancy across different Na sites was applied to the refinement according to stoichiometric values.

Table S5: Crystallographic information for P2 and O'3-type NZTO obtained from Rietveld refinement against SPXRD data of NZTO700. P2-type phase in space group $P6_322$ (*No*.182), $a = b = 5.2747^a$ and $c = 11.242^a$ Å, $V = 270.86^a$ Å^3; O'3-type phase (based on O'3_model_2) in space group *C2/m* (*No*.12), $a = 5.321(2)$, $b = 9.183(3)$ and $c = 5.861(2)$ Å, $\beta = 109.13(2)°$, $V = 270.6(2)$ Å^3, $R_{wp} = 10.34\%$, $R_{exp} = 8.14\%$, GOF = 1.27.

Atom	Wyckoff Symbol	Coordinates			B_{iso} (Å^2)	Occupancy
		x	*y*	*z*		
P2-type phase (~54%)						
Na1	6*g*	0.61[a]	0	0	2.1[a]	0.43[a]
Na2	2*a*	0	0	0	2.1[a]	0.00[a]
Na3	4*f*	1/3	2/3	0.462[a]	2.1[a]	0.35[a]
O1	12*i*	0.352[a]	0.359[a]	0.652[a]	1.5[a]	1
Zn1	2*b*	0	0	1/4	1.0[a]	1
Zn2	2*d*	1/3	2/3	3/4	1.0[a]	1
Te1	2*c*	1/3	2/3	1/4	1.0[a]	1
O'3-type phase (~44%)						
Na1	2*d*	0	1/2	1/2	2.1[a]	0.59(6)[c]
Na2	4*h*	1/2	0.33(1)	1/2	2.1[a]	0.71(3)[c]
O1	8*j*	0.221(7)	0.830(7)	0.214(6)	1.5[a]	1
O2	4*i*	0.26(1)	1/2	0.20(1)	1.5[a]	1
Zn1	4*g*	0	2/3	0	1.0[a]	0.94(1)[c]
Zn2	2*a*	0	0	0	1.0[a]	0.12(3)[c]
Te1	2*a*	0	0	0	1.0[a]	0.88(3)[c]
Te2	4g	0	2/3	0	1.0[a]	0.06(1)[c]

[a]B_{iso} values are fixed at values obtained from NZTO900 refinement; [a]structure-related parameters for P2-type phase are fixed according to the NZTO700 refinement based on O'3_model_1; 16 structure-related parameters for O'3-type phase including lattice parameters, atomic coordinates and occupancies were refined; [c]constraints of total occupancy across different Na sites, Zn sites and Te sites were applied to the refinement according to stoichiometric values.

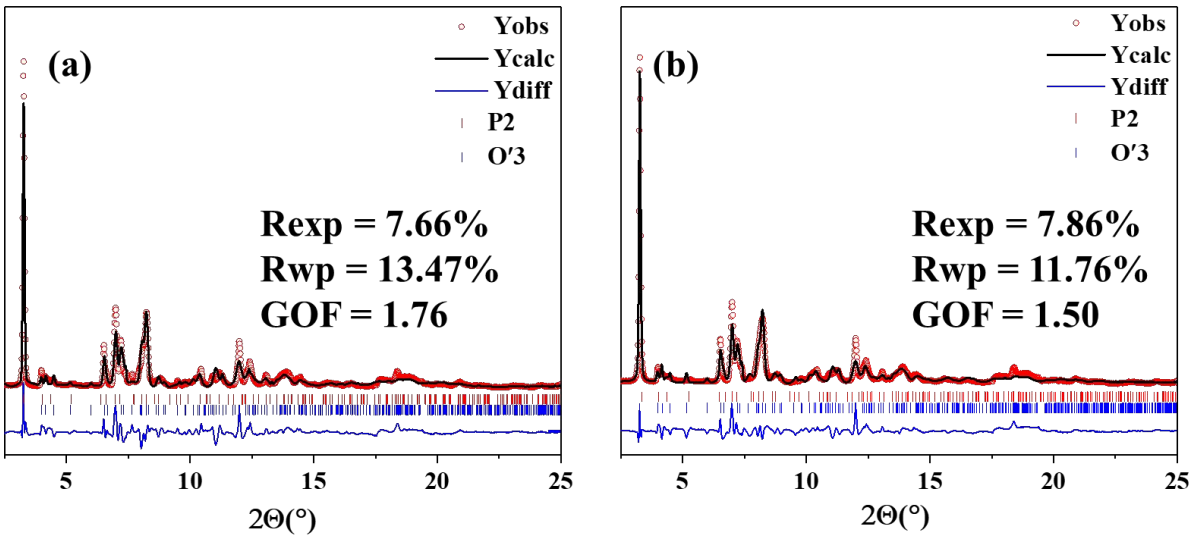

Figure S5: Rietveld refinements against SPXRD data of (a) NZTO600 and (b) NZTO500 based on O'3_model_2. The experimental pattern is shown in red, calculated pattern in black, the difference between experimental and calculated curves in blue. Bragg positions of P2 and O'3-type phases are in red and blue, respectively. Wavelength (λ) for both SPXRD patterns is 0.319089 Å.

Table S6: Fraction of P2 and O'3-type phases in respective NZTO500-900 samples.

Phase Fraction (%)	NZTO500	NZTO600	NZTO700	NZTO800	NZTO900
P2	6.5(5)	10.5(4)	53.9(4)	92.0(3)	100
O'3	91.5(5)	87.2(4)	43.8(4)	6.2(3)	0

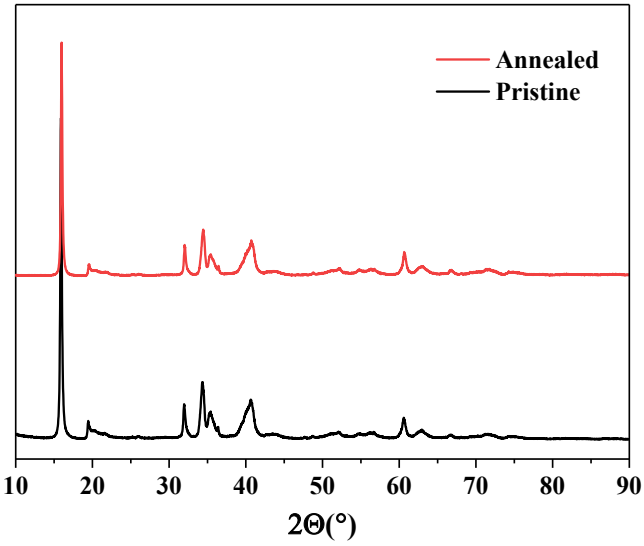

Figure S6: PXRD patterns of pristine and annealed NZTO500 samples, λ = 1.5406 Å (Annealing: 500 ºC for 7 days)

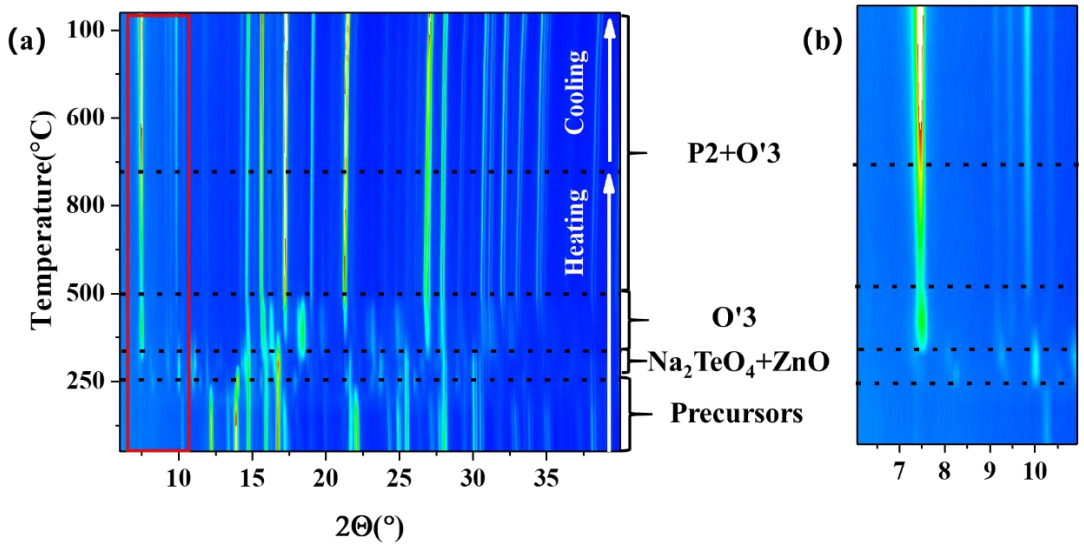

Figure S7: (a) 2D contour plot showing the temperature dependence of XRD patterns indicating phase evolution during calcination process and sequential cooling process within temperature range of 30-900 ºC (b) enlargement of 2θ range 6 - 11°.

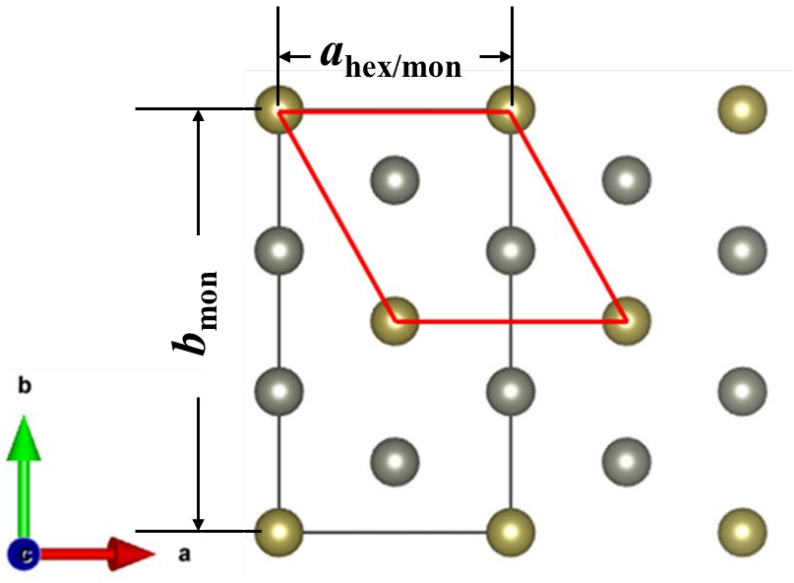

$$a_{hex} = b_{hex}$$

$$a_{hex} = a_{mon}$$

$$b_{mon} = \sqrt{3}a_{hex}$$

Figure S8: Spatial relationship between the monoclinic *C2/m* (black) unit cell for O'3-type phase and the hexagonal $P6_322$(red) unit cell for P2-type phase.

Table S7: Nearest and next nearest neighbours shells for Na atoms in the O'3-type structure.

Na sites	Shell 1		Shell 2		
2*d*	Te (3.25 Å)	Zn (3.30 Å)	Zn (3.30 Å)	Zn (4.46 Å)	Zn (4.46 Å)
4*h*	Zn (3.24 Å)	Te (3.29 Å)	Zn (3.31 Å)	Zn (4.44 Å)	Te (4.49 Å)

Table S8: Sodium occupancy and fitting parameters to the equation of state for the considered NZTO configurations.

Structure	Na occ.	*E*(eV)	V(Å^3)	B(GPa)	B’
O'3	4*h*	0.00	136.10	83.1	3.5
O'3	2*h*2*d*	0.04	136.27	82.0	4.4
P2	2*f*2*f*	0.04	140.21	74.9	5.0
P2	4*g*	0.1	137.59	81.5	4.1

While the previous calculations clearly indicate the O'3 the most likely secondary phase to coexist with the P2-type structure, they do not provide definitive proof of its stability as single phase. To provide conclusive evidence of its existence we have calculated the phonon density of states and the elastic constants respectively. Analogous calculations were also performed for the P2-type phase and are shown for comparison.

The vibrational densities of states are reported in Figure S9. Imaginary frequencies are absent for both the P2 and the O'3-type phases, thus confirming their dynamical stability. While the vibrational properties of Te, Zn and O do not significantly change across the two phases, the density of states for Na presents an extra peak at low frequency (~2 Thz). Since the center of the phononic density of states is correlated to the activation energy for Na^+ ion mobility[1], this feature is in line with the better mobility of the P2-type phase over the O'3.

Finally, the elastic constant matrix is calculated and diagonalized. The complete tensors are reported in Table S9. All the eigenvalues, shown in Table S10 are positive and thus the general condition for mechanical stability is also verified.

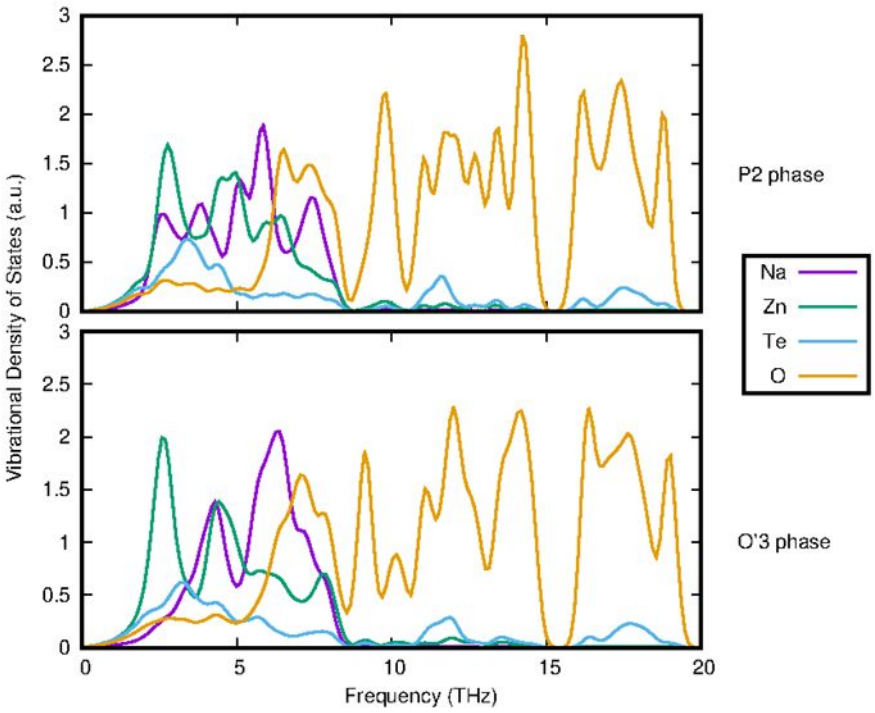

Figure S9: Vibrational atom-resolved density of states for P2 and O'3-type NZTO.

Table S9: Elastic constants tensor calculated for P2 and O'3-type NZTO.

P2						O'3					
203	80	23	-0	0	0	155	83	32	22	-0	0
80	180	20	-0	0	-0	83	228	28	9	0	-0
23	20	128	0	0	0	32	28	121	11	0	-0
-0	-0	0	22	-0	0	22	9	11	31	0	0
0	0	0	-0	9	-0	-0	0	0	0	26	5
0	-0	0	0	-0	37	0	-0	-0	0	5	53

The fitting parameters to the Murnaghan equation of states for the considered phases are reported in Table S10. Energies are reported per formula unit, using the energy of the most stable O'3-type phase as reference. As detailed in the main text, the two O'3-type phases and the non-hexagonal P2 one are close in energy. The latter stabilizes at a larger volume and can, therefore, be obtained by high-temperature synthesis, as thoroughly explained in the main text. The P2 phase with Na at g sites is energetically unfavorable.

The values for the bulk modulus are clearly correlated to the equilibrium volumes: more compact structures are, clearly, more resistant to elastic deformation. In the reconstructed P2-type phase its value is considerably smaller (~10% smaller than the other 3 considered configurations). This is because this is the only configuration in which face-sharing of coordination polyhedra (NaO_6 triangular prism and TeO_6, NaO_6 octahedra) is present.

Table S10: Eigenvalues of the elastic constants tensor calculated for P2 and O'3-type NZTO.

Phases	λ_1	λ_2	λ_3	λ_4	λ_5	λ_6
P2	279	122	111	37	22	9
O'3	294	119	95	54	26	26

Table S11: Elemental analysis for $Na_{2+x}Zn_{2-x}Li_xTeO_6$ (x = 0, 0.1, 0.2 and 0.5) obtained from ICP measurements.

Element	Molar fraction			
	$Na_2Zn_2TeO_6$	$Na_{2.1}Zn_{1.9}Li_{0.1}TeO_6$	$Na_{2.2}Zn_{1.8}Li_{0.2}TeO_6$	$Na_{2.5}Zn_{1.5}Li_{0.5}TeO_6$
Na	2.03	2.13	2.24	2.51
Zn	2.01	1.91	1.79	1.49
Li	0	0.1	0.21	0.51
Te	1	1	1	1

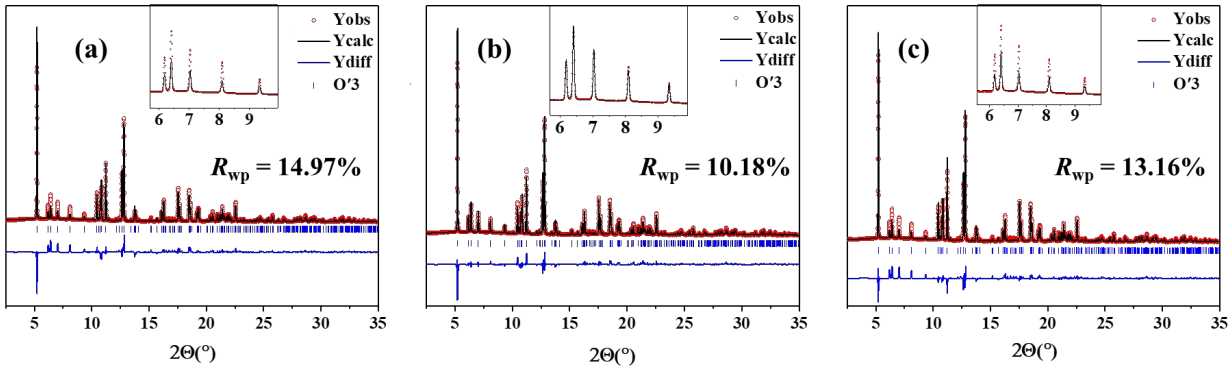

Figure S10: Rietveld refinements against SPXRD data of $Na_{2.5}Zn_{1.5}Li_{0.5}TeO_6$: (a) test 1; (b) test2; (c) test3. (Insets: enlargement of 2θ range of 5.5 to 9.8°) The experimental pattern is shown in red, calculated pattern in black, the difference between experimental and calculated curves in blue. Bragg positions of O'3-type phase are in blue. Wavelength (λ) for both SPXRD patterns is 0.49426 Å.

In order to identify the Li position in Li-doped NZTO, we then performed four individual tests using Rietveld refinement against data of $Na_{2.5}Zn_{1.5}Li_{0.5}TeO_6$ due to its highest Li-content among three Li-doped samples and corresponding refinements are presented in Figure S10. All these refinements were performed using O'3_model_2 as starting model and the total Te site occupancies were fixed to stoichiometric value. In the first test, total site occupancies for Na and Zn were fixed to their stoichiometric values for NZTO by constraints, only lattice

parameters and scale factor were refined. The peak intensities are not well described especially at low angle region. In the second test, we freely refined Zn site occupancies which indicates a total Zn occupancies across 4*g* and 2*a* sites close to 1.5/formula. The imperfectly described peak intensities in the first test were well described in this case. We further allowed Na site occupancies to refine freely in the third test. The refinement indicates a total Na occupancies across 2*d* and 4*h* sites close to 2.65/formula, peak intensities not well described.

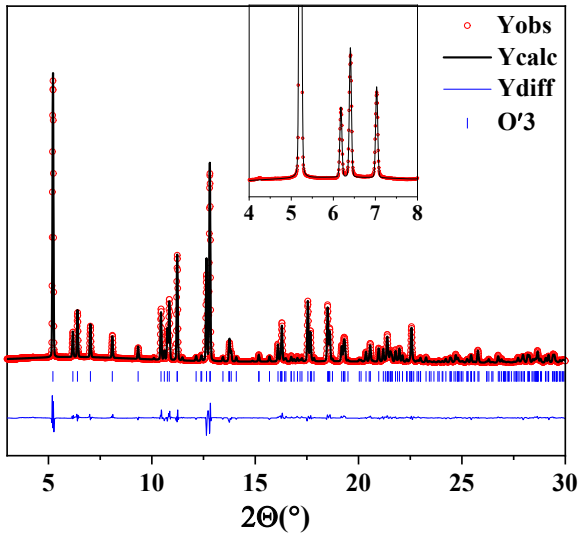

Figure S11: Rietveld refinement against SPXRD data of $Na_{2.5}Zn_{1.5}Li_{0.5}TeO_6$ based on O'3_model_2 (test 4). (Inset: enlargement of 2θ range of 4 to 8°) The experimental pattern is shown in red, calculated pattern in black, the difference between experimental and calculated curves in blue. Bragg positions of O'3-type phase is in blue. Wavelength (λ) for both SPXRD patterns is 0.49426 Å.

Table S12: Crystallographic information for O'3-type phase obtained from Rietveld refinement against SPXRD data of $Na_{2.5}Zn_{1.5}Li_{0.5}TeO_6$. Space group *C2/m*, unit cell parameters: a = 5.3352(1), b = 9.1714(2) and c = 5.7370(1) Å, β = 108.774(1)°, V = 265.78(1) Å^3. Discrepancy factors: R_{wp} = 8.34%, R_{exp} = 29.20%, GOF = 0.29.

Atom	Wyckoff Symbol	Coordinates			B_{iso} (Å^2)	Occupancy
		x	*y*	*z*		
Na1	2*d*	0	1/2	1/2	2.1[a]	0.802(7)[c]
Na2	4*h*	1/2	0.3330(7)	1/2	2.1[a]	0.849(4)[c]
O1	8*j*	0.2268(8)	0.8433(5)	0.2056(6)	1.5[a]	1[a]
O2	4*i*	0.252(1)	1/2	0.210(1)	1.5[a]	1[a]
Zn1	4*g*	0	2/3	0	1.0[a]	0.739(2)[c]
Zn2	2*a*	0	0	0	1.0[a]	0.023(4)[c]
Te1	2*a*	0	0	0	1.0[a]	0.977(4)[c]
Te2	4*g*	0	2/3	0	1.0[a]	0.011(2)[c]
Li1	4*g*	0	2/3	0	2.1[a]	0.250(2)[a]

[a]B_{iso} values are fixed at values obtained from NZTO900 refinement; [b]17 structure-related parameters for O'3-type phase including lattice parameters, atomic coordinates, Na site, Zn and Te occupancies were refined; [c]constraints of total occupancy across difference Na sites, Zn sites and Te sites were applied to the refinement according to stoichiometric values.

Table S13: Crystallographic information for P2 and O'3-type phases obtained from Rietveld refinement against SXRD data of $Na_{2.1}Zn_{1.9}Li_{0.1}TeO_6$. P2-type phase in space group $P6_322$ (*No.*182), $a = b = 5.2803(1)$ and $c = 11.2128(2)$ Å, $V = 270.75(1)$ Å^3; O'3-type phase (based on O'3_model_2) in space group $C2/m$ (*No.*12), $a = 5.3346(7)$, $b = 9.198(1)$ and $c = 5.8209(5)$ Å, $\beta = 109.05(1)°$, $V = 270.00(6)$ Å^3, $R_{wp} = 9.84\%$, $R_{exp} = 32.42\%$, GOF = 0.30.

Atom	Wyckoff Symbol	Coordinates			B_{iso} (Å^2)	Occupancy
		x	*y*	*z*		
P2-type phase (~90%)						
Na1	6*g*	0.662(3)	0	0	1[a]	0.476(4)[c]
Na2	2*a*	0	0	0	1[a]	0.10(1)[c]
Na3	4*f*	1/3	2/3	0.512(2)	1[a]	0.285(9)[c]
O1	12*i*	0.342(1)	0.331(1)	0.6477(3)	1[a]	1[a]
Zn1	2*b*	0	0	1/4	1[a]	0.938(3)[c]
Zn2	2*d*	1/3	2/3	3/4	1[a]	0.962(3)[c]
Li1	2*b*	0	0	1/4	1[a]	0.062(3)[c]
Li2	2*d*	1/3	2/3	3/4	1[a]	0.038(3)[c]
Te1	2*c*	1/3	2/3	1/4	1[a]	1[a]
O'3-type phase (~9%)						
Na1	2*d*	0	1/2	1/2	2.1[a]	0.65[a]
Na2	4*h*	1/2	0.333[a]	1/2	2.1[a]	0.725[a]
O1	8*j*	0.229[a]	0.8433[a]	0.2009[a]	1.5[a]	1[a]
O2	4*i*	0.252[a]	1/2	0.210[a]	1.5[a]	1[a]
Zn1	4*g*	0	2/3	0	1.0[a]	0.950[a]
Zn2	2*a*	0	0	0	1.0[a]	0.000[a]
Te1	2*a*	0	0	0	1.0[a]	1.000[a]
Te2	4*g*	0	2/3	0	1.0[a]	0.000[a]
Li1	4*g*	0	2/3	0	2.1[a]	0.05[a]

[a]B_{iso} values are fixed at values obtained from NZTO900 refinement; [a]structure-related parameters for O'3-type phase are fixed according to the $Na_{2.2}Zn_{1.8}Li_{0.2}TeO_6$ refinement based on O'3_model_2; 10 structure-related parameters for P2-type phase including lattice parameters, atomic coordinates and Na site occupancies were refined; [c]a constraint of total occupancy across different Na sites was applied to the refinement according to stoichiometric values.

Table S14: Crystallographic information for O'3-type $Na_{2.2}Zn_{1.8}Li_{0.2}TeO_6$ from Rietveld refinement against SPXRD data. Space group *C2/m*, unit cell parameters: a = 5.3181(1), b = 9.1842(2) and c = 5.8215(2) Å, β = 108.920(2)°, V = 268.97(1) Å^3. Discrepancy factors: R_{wp} = 9.98%, R_{exp} = 31.64%, GOF = 0.32.

Atom	Wyckoff Symbol	Coordinates[a]			B_{iso} (Å^2)	Occupancy
		x	*y*	*z*		
Na1	2*d*	0	1/2	1/2	2.1[a]	0.80(1)[c]
Na2	4*h*	1/2	0.333(1)	1/2	2.1[a]	0.802(5)[c]
O1	8*j*	0.229(1)	0.8433(7)	0.2009(8)	1.5[a]	1[a]
O2	4*i*	0.252(2)	1/2	0.210(1)	1.5[a]	1[a]
Zn1	4*g*	0	2/3	0	1.0[a]	0.900(3)[c]
Zn2	2*a*	0	0	0	1.0[a]	0.000(6)[c]
Te1	2*a*	0	0	0	1.0[a]	1.000(6)[c]
Te2	4*g*	0	2/3	0	1.0[a]	0.000(3)[c]
Li1	4*g*	0	2/3	0	2.1[a]	0.100(3)[c]

[a]B_{iso} values are fixed at values obtained from NZTO900 refinement; [b]17 structure-related parameters for O'3-type phase including lattice parameters, atomic coordinates, Na site, Zn and Te occupancies were refined; [c]constraints of total occupancy across difference Na sites, Zn sites and Te sites were applied to the refinement according to stoichiometric values.

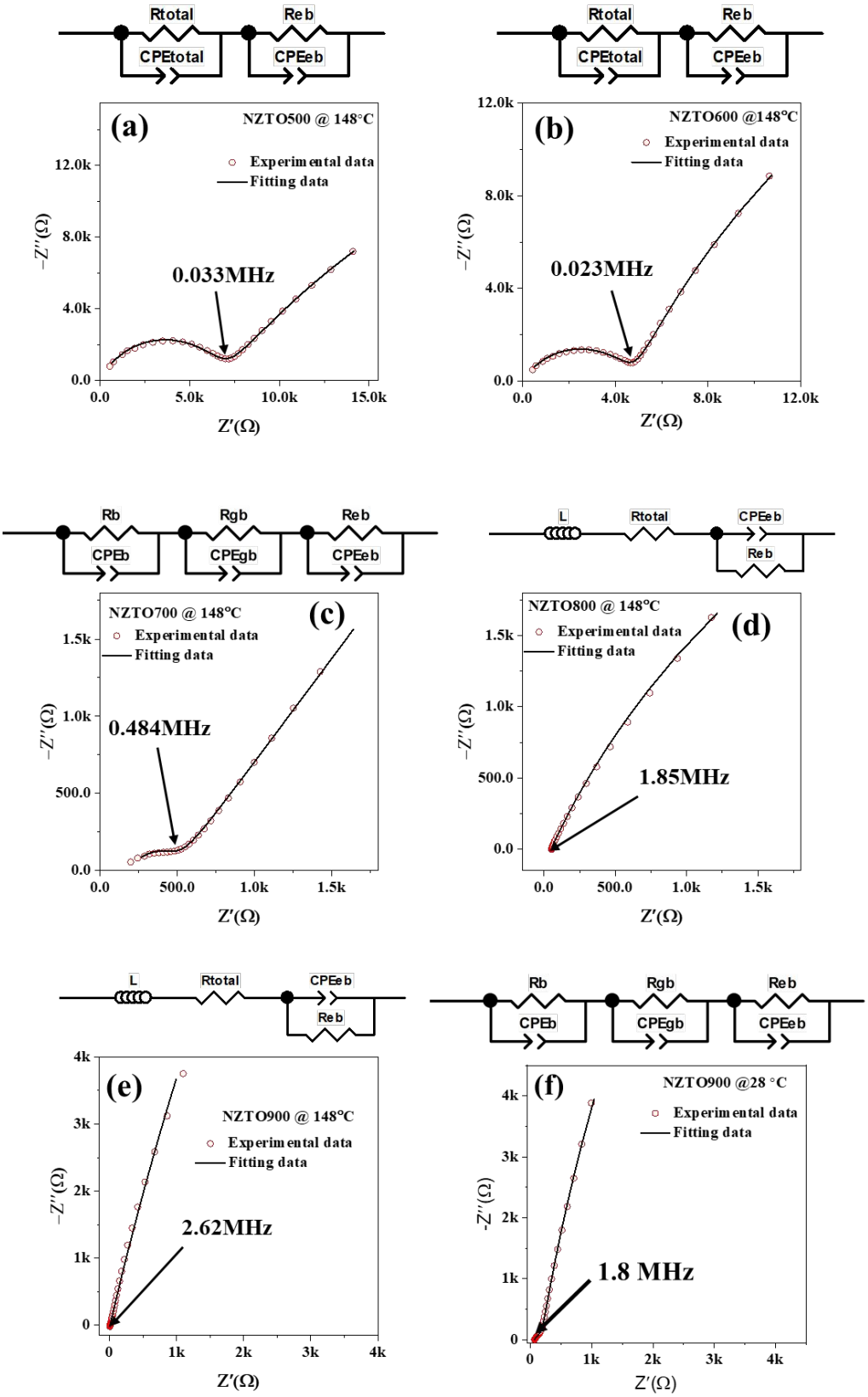

Figure S12: Nyquist plots of (a) NZT0500, (b) NZTO600, (c) NZTO700, (d) NZTO800, (e) NZTO900 measured at 148 °C and (f) NZTO900 measured at 28 °C with experimental data (symbols) and fitting data (solid line) obtained from fit to equivalent circuit on the top of each graph.

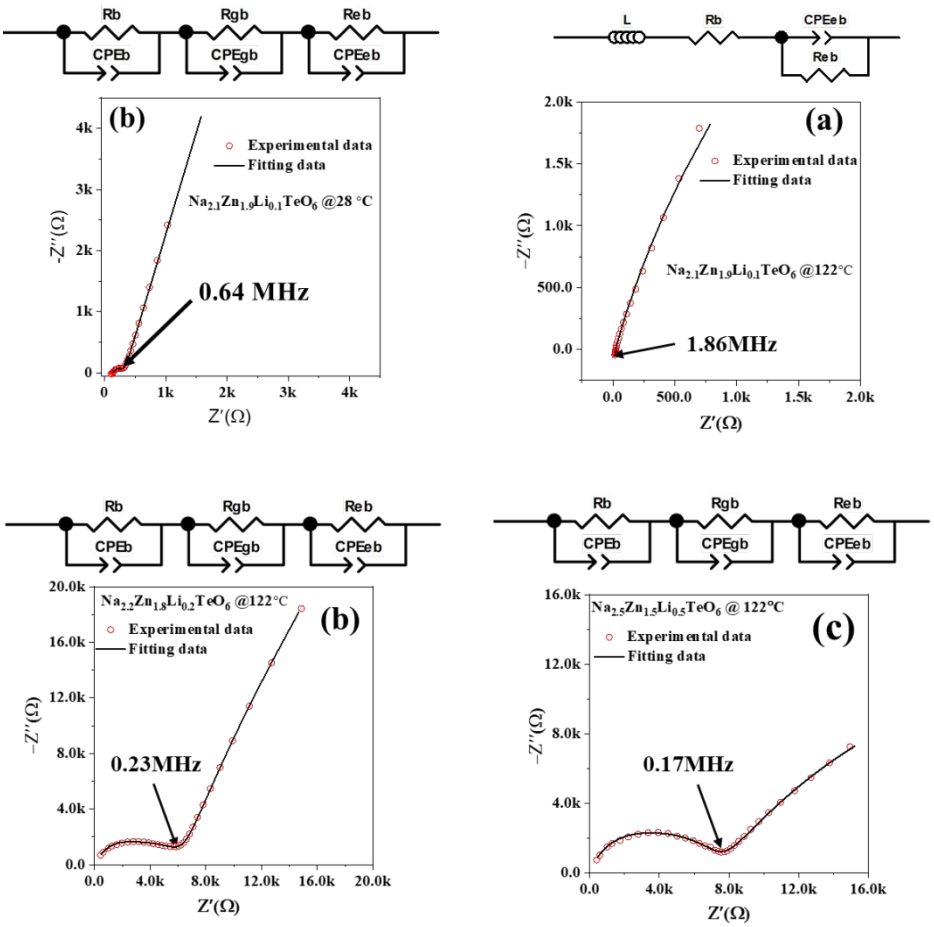

Figure S13: Nyquist plots of (a) $Na_{2.1}Zn_{1.9}Li_{0.1}TeO_6$ measured at 28 °C and (b) $Na_{2.1}Zn_{1.9}Li_{0.1}TeO_6$, (c) $Na_{2.2}Zn_{1.8}Li_{0.2}TeO_6$, (d) $Na_{2.5}Zn_{1.5}Li_{0.5}TeO_6$ measured at 122 °C with experimental data (symbols) and fitting data (solid line) obtained from fit to equivalent circuit on the top of each graph.

Table S15: Comparison of Na^+ ion conductivities σ (S/cm) at 25 °C and activation energies E_a for NZTO500-900 and Li-doped NZTO samples. O'3-type phase fractions in corresponding samples are listed for comparison.

Samples	σ (S/cm)	E_a (eV)	O'3 Phase Fraction (%)
NZTO500	$(0.52 – 1.88) \times 10^{-7}$	0.56(2) (148-211 °C)	91.5(5)
NZTO600	$(5.23 - 10) \times 10^{-7}$	0.53(7) (148-211 °C)	87.2(4)
NZTO700	$(2.83 – 4.61) \times 10^{-6}$	0.43(2) (101-211 °C)	43.8(4)
NZTO800	$(2.27 – 2.71) \times 10^{-4}$	0.300(6) (52-211°C)	6.2(3)
NZTO900	$(3.55 – 4.21) \times 10^{-4}$	0.289(6) (28-211 °C)	0
$Na_{2.1}Zn_{1.9}Li_{0.1}TeO_6$	$(3.79 – 4.29) \times 10^{-4}$	0.299(4) (28-211 °C)	9.20(1)
$Na_{2.2}Zn_{1.8}Li_{0.2}TeO_6$	$(1.57 – 7.32) \times 10^{-8}$	0.68(2) (122-211 °C)	100
$Na_{2.5}Zn_{1.5}Li_{0.5}TeO_6$	$(0.79 – 10.5) \times 10^{-8}$	0.68(6) (122-211 °C)	100

Table S16: Ionic conductivities and activation energies for $Na_2M_2TeO_6$ (M = Zn, Mg, Co, Ni) from this work and literature.

Compound	σ (S/cm) @25 °C	E_a (eV)	reference
P2-$Na_2Zn_2TeO_6$	$(3.55 – 4.21) \times 10^{-4}$	0.289(6) (28 – 211 °C)	This work
P2-$Na_2Zn_2TeO_6$	9×10^{-5}	--	[2]
P2-$Na_2Zn_2TeO_6$	6.29×10^{-4}	0.327 (50 – 120 °C)	[3]
P2-$Na_{1.9}Zn_{1.9}Ga_{0.1}TeO_6$	1.09×10^{-3}	0.271 (50 – 120 °C)	[3]
P2-$Na_2Zn_{1.98}Ca_{0.02}TeO_6$	7.54×10^{-4}	0.225 (50 – 120 °C)	[4]
P2-$Na_2Mg_2TeO_6$	6.3×10^{-5}	--	[2]
P2-$Na_2Mg_2TeO_6$	2.3×10^{-4}	0.341 (50 – 120 °C)	[5]
P2-$Na_2Ni_2TeO_6$	$(0.8 – 3.4) \times 10^{-5}$	0.553 (100 – 350 °C)	[2]
P2-$Na_{1.9}Ni_{1.9}Fe_{0.1}TeO_6$	1×10^{-4}	0.381 (100 –350 °C)	[2]
P2-$Na_2Co_2TeO_6$	$(3.8 – 4.9) \times 10^{-6}$	0.524 (100 – 350 °C)	[2]
O'3-$Na_{2.5}Zn_{1.5}Li_{0.5}TeO_6$	$(0.79 – 10.5) \times 10^{-8}$	0.68(6) (122 – 211 °C)	This work

Reference

(1) Muy, S.; Voss, J.; Schlem, R.; Koerver, R.; Sedlmaier, S. J.; Maglia, F.; Lamp, P.; Zeier, W. G.; Shao-Horn, Y. High-Throughput Screening of Solid-State Li-Ion Conductors Using Lattice-Dynamics Descriptors. *iScience* **2019,** *16*, 270-282.

(2) Evstigneeva, M. A.; Nalbandyan, V. B.; Petrenko, A. A.; Medvedev, B. S.; Kataev, A. A. A New Family of Fast Sodium Ion Conductors: $Na_2M_2TeO_6$ (M = Ni, Co, Zn, Mg). *Chem. Mater.* **2011,** *23*, 1174-1181.

(3) Li, Y.; Deng, Z.; Peng, J.; Chen, E.; Yu, Y.; Li, X.; Luo, J.; Huang, Y.; Zhu, J.; Fang, C.; Li, Q.; Han, J.; Huang, Y. A P2-Type Layered Superionic Conductor Ga-Doped $Na_2Zn_2TeO_6$ for All-Solid-State Sodium-Ion Batteries. *Chem. Eur. J.* **2018,** *24*, 1057-1061.

(4) Deng, Z.; Gu, J.; Li, Y.; Li, S.; Peng, J.; Li, X.; Luo, J.; Huang, Y.; Fang, C.; Li, Q.; Han, J.; Huang, Y.; Zhao, Y. Ca-Doped $Na_2Zn_2TeO_6$ Layered Sodium Conductor for All-Solid-State Sodium-Ion Batteries. *Electrochim. Acta* **2019,** *298*, 121-126.

(5) Li, Y.; Deng, Z.; Peng, J.; Gu, J.; Chen, E.; Yu, Y.; Wu, J.; Li, X.; Luo, J.; Huang, Y.; Xu, Y.; Gao, Z.; Fang, C.; Zhu, J.; Li, Q.; Han, J.; Huang, Y. New P2-Type Honeycomb-Layered Sodium-Ion Conductor: $Na_2Mg_2TeO_6$. *ACS Appl. Mater. Interfaces* **2018,** *10*, 15760-15766.